Impact of the primordial fluctuation power spectrum on the reionization history

Teppei Minoda[1] Shintaro Yoshiura,[2] and Tomo Takahashi[3]

[1]*Tsinghua University, Department of Astronomy, Beijing 100084, China*
[2]*Mizusawa VLBI Observatory, National Astronomical Observatory Japan,*
2-21-1 Osawa, Mitaka, Tokyo 181-8588, Japan
[3]*Department of Physics, Saga University, Saga 840-8502, Japan*

We argue that observations of the reionization history can be used as a probe of primordial density fluctuations, particularly on small scales. Although the primordial curvature perturbations are well constrained from measurements of cosmic microwave background (CMB) anisotropies and large-scale structure, these observational data probe the curvature perturbations only on large scales, and hence, its information on smaller scales will give us further insight on primordial fluctuations. Since the formation of early galaxies is sensitive to the amplitude of small-scale perturbations, and then, in turn, gives an impact on the reionization history, one can probe the primordial power spectrum on small scales through observations of reionization. In this work, we focus on the running spectral indices of the primordial power spectrum to characterize the small-scale perturbations and investigate their impact on the reionization history using the numerical code 21cmFAST, which adopts a simple but commonly used reionization model. We also derive the constraints on the running spectral indices from observations of the reionization history indicated by the luminosity function of the Lyman-α emitters. We show that the reionization history, in combination with large-scale observations such as CMB, would be a useful tool to investigate primordial density fluctuations.

I. INTRODUCTION

The statistical property of primordial perturbations is well understood by measurements of cosmic microwave background (CMB) [1] and large-scale structure (LSS) [2–7] in this decade. The perturbations are almost adiabatic and Gaussian. The power spectrum of the primordial perturbations is nearly scale invariant, but slightly red tilted. These characteristics of the primordial perturbations provide strong constraints on inflation and their generation mechanism.

The scale dependence of primordial power spectrum $\mathcal{P}_\zeta$ is usually characterized by a constant spectral index n_s with which the power spectrum is given by

$$\mathcal{P}_\zeta \propto k^{n_s-1}. \qquad (1.1)$$

However, in usual inflation models, n_s is not exactly constant but has some scale dependence, and in some cases, it can be strongly scale dependent. Such a scale dependence is commonly characterized by the so-called "runnings" in which the power spectrum is represented by

$$\mathcal{P}_\zeta \propto k^{n_s-1+\frac{1}{2}\alpha_s \ln(k/k_0)+\frac{1}{6}\beta_s[\ln(k/k_0)]^2}, \qquad (1.2)$$

with α_s and β_s being denoted as running parameters at the pivot scale k_0. Because observations such as CMB and LSS

probe the primordial fluctuations only on large scales as 10^{-3} Mpc$^{-1} \lesssim k \lesssim 1$ Mpc^{-1} [1], we need to investigate the fluctuations on different scales in order to study the scale dependence of the primordial fluctuations further. Indeed, there have been many attempts to investigate fluctuations on small scales $k \gtrsim 1$ Mpc^{-1} to probe primordial fluctuations using observations such as the 21-cm global signal [8,9], 21-cm power spectrum [10,11], 21-cm forest [12], Lyman-α forest [13,14], 21-cm signal from minihalos [15], ultracompact minihalos [16,17], primordial black holes formation [18,19], supernovae lensing [20], spectral distortions of CMB [21–27], galaxy UV luminosity function [28], the substructure of dark matter halo [29], and so on.

Our approach in this paper is to study the impact of the primordial power spectrum on the reionization history. Since fluctuations on small scales $k \gtrsim 1$ Mpc^{-1} are connected to the halos with mass $M \lesssim 10^{11} M_\odot$, which are expected to be formed around the cosmic dawn and the epoch of reionization, thereby we can utilize observations of the reionization history as a probe of such small-scale primordial fluctuations. One famous cosmological constraint on the reionization history is the Thomson optical depth of CMB, which corresponds to the column density of the free electron. Therefore, it provides the redshift-integrated information on the reionization history. We can

also probe the reionization physics from observations of the Lyman-α emitter (LAE) luminosity function, which gives the redshift-dependent information on the reionization history. We focus on the latter observation to probe the primordial fluctuations from the reionization history by using a simple and widely used numerical calculation code 21cmFAST. In particular, we use reionization history estimated by the SILVERRUSH survey data with the Subaru telescope [30], from which we can constrain the running of the spectral index α_s and β_s.

In the following, we first introduce observational constraints on the reionization history in Sec. II A and our method to calculate the evolution of the free electron fraction in Sec. II B. Then in Sec. II C, we provide the constraints on the runnings of the primordial power spectrum from observations of the reionization. We conclude and summarize this paper in Sec. III. In our analysis, we fix the cosmological parameters, other than the runnings of the spectral index, as $\sigma_8 = 0.831$, $H_0 = 67.27$ km/s/Mpc, $\Omega_m = 0.32$, $\Omega_b = 0.049$, and $n_s = 0.9586$, assuming the flat ΛCDM cosmology [31].

II. REIONIZATION HISTORY AS A PROBE OF PRIMORDIAL FLUCTUATIONS

A. Observational constraint on the reionization history

In this work, we put a constraint on the running parameters of the primordial power spectrum from observations of the Ly-α luminosity function with SILVERRUSH by calculating the reionization history [30]. Indeed one can also use the measurement of the CMB optical depth from Planck [32] to obtain the constraint. However, as we show in the following, the constraint on the optical depth from the Ly-α luminosity function with SILVERRUSH is tighter than that from CMB, and hence, we focus on the constraint from the reionization history (more specifically the value of x_e at some redshift) estimated by the Ly-α luminosity function. Firstly, by using a simple tanh-type reionization model, we demonstrate how the reionization history is constrained by the latest Planck and SILVERRUSH data. The free electron fraction at a given redshift z is often modeled by the hyperbolic tangent function as [33]

$$x_e(z, z_{re}) = \frac{1}{2}\left[1 + \tanh\left(\frac{y(z_{re}) - y(z)}{\Delta y}\right)\right], \quad (2.1)$$

where z_{re} is the model parameter that represents the central redshift of reionization, and $y(z) = (1+z)^{2/3}$, $\Delta y = 3/2(1+z_{re})^{1/2}\Delta z$, with $\Delta z = 0.5$. We note that although the redshift width of reionization Δz is in general considered to be a free parameter as assumed in the original reference [33], we fix it as $\Delta z = 0.5$ in most of our analyses since this width fits the SILVERRUSH results well and the recent Planck analysis also assumes $\Delta z = 0.5$ [32]. Only in Sec. II D, we vary Δz to argue that the width Δz does not actually affect the constraints very much.
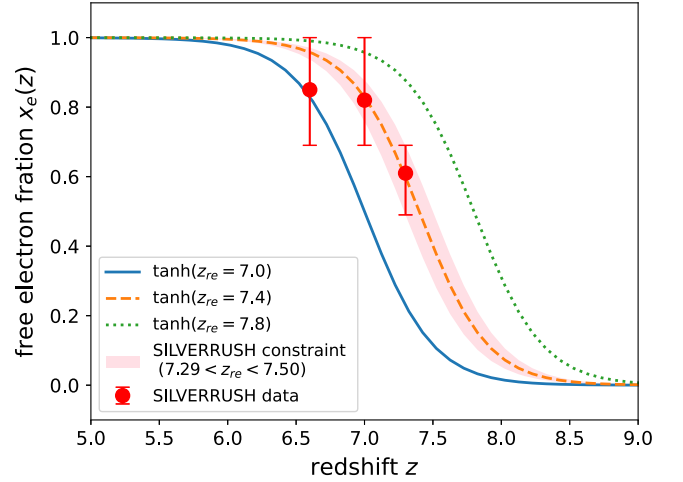
FIG. 1. Redshift evolution of the free electron fraction with $z_{re} = 7.0$ (solid), 7.4 (dashed), and 7.8 (dotted). Three red points at $z = 6.6$, 7.0, and 7.3 are the SILVERRUSH results, given in Table 2 of Ref. [30]. The pink-shaded region corresponds to the range of x_e from the constraint of the SILVERRUSH results for the tanh-type reionization model with $7.29 \leq z_{re} \leq 7.50$.

Figure 1 shows the tanh-type reionization history for different z_{re}, together with the constraint on the free electron fraction from the SILVERRUSH results of the Ly-α luminosity function. Three data points from the SILVERRUSH results are depicted in the figure. The most stringent constraint among them is $0.49 \leq x_e \leq 0.69$ at $z = 7.3$. This constraint can be translated into that on the central redshift of the reionization z_{re} as $7.29 \leq z_{re} \leq 7.50$ for the modeling of x_e given in Eq. (2.1). The corresponding range for x_e is shown with the pink-shaded region in Fig. 1. We note that, even when we change the redshift width of the reionization as $\Delta z = 1.0$, the constraint on the central redshift of reionization is given by $7.42 \leq z_{re} \leq 7.70$, which is consistent with that for the case of $\Delta z = 0.5$. Therefore, the change of Δz does not give a significant impact on our conclusion. We show the case of varied Δz in Sec. II D.

Other SILVERRUSH data points, $x_e \geq 0.69$ at $z = 7.0$ and $x_e \geq 0.69$ at $z = 6.6$, can be translated into $z_{re} \geq 7.20$ and $z_{re} \geq 6.80$, respectively. These constraints are weaker than that from the data point at $z = 7.3$, so we do not use two data points at $z = 7.0$ and 6.6 in the following analysis unless explicitly mentioned.

To compare the constraint from SILVERRUSH with that from the Planck optical depth, we calculate the Thomson optical depth, which is obtained by integrating the tanh-type reionization history, via

$$\tau = n_H c \sigma_T \int_0^{z_{max}} dz\, x_e(z, z_{re}) \frac{(1+z)^2}{H(z)}, \quad (2.2)$$

with the number density of hydrogen n_H, the speed of light c, the Thomson scattering cross-section σ_T, and the Hubble parameter $H(z)$. As referred in [32], we take the maximum redshift in the integration as $z_{max} = 50$. We show
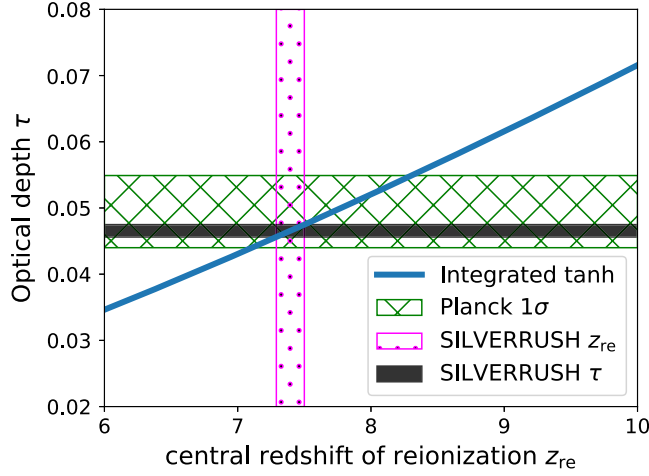
FIG. 2. Thomson optical depth obtained by Eq. (2.2) with the tanh-type reionization history, as a function of z_{re} (the blue thick line). The green cross-hatched horizontal region is the constraint on the optical depth from Planck 2018 results. The magenta dot-hatched vertical one is obtained by the tanh-type reionization history with the SILVERRUSH results, as $7.29 \leq z_{re} \leq 7.50$. The horizontal thick-shaded region corresponds to the range of τ suggested from the SILVERRUSH constraints on z_{re} for the tanh-type reionization model.

the Thomson optical depth from the tanh-type reionization with different z_{re} in Fig. 2. The SILVERRUSH constraint on the central redshift of the reionization is $7.29 \leq z_{re} \leq 7.50$ and plotted with the dot-hatched region in Fig. 2. Assuming the tanh-type reionization history, this constraint on z_{re} can be translated to the constraint on the Thomson optical depth, as $0.0456 \leq \tau \leq 0.0475$, which is obtained from the overlapping range between the blue thick line and the magenta dot-hatched region. This constraint on τ is plotted with the horizontal thick-shaded region. For comparison, we also show the Planck constraint on the optical depth, $0.0440 \leq \tau \leq 0.0549$ given in Eq. (86a) in Ref. [32] with the horizontal green cross-hatched region. It is clear that the SILVERRUSH constraint is stronger than the Planck one when we assume the tanh-type reionization.

B. Reionization calculation with the 21cmFAST

We adopt the publicly available seminumerical simulation code 21cmFAST [34] to calculate the reionization history. We modify the code to extend the cosmological model in 21cmFAST, to include the "running" and "running of running" of the primordial curvature power spectrum, α_s and β_s as

$$\mathcal{P}_\zeta(k) = A_s \left(\frac{k}{k_0}\right)^{n_s - 1 + \frac{1}{2}\alpha_s \ln(\frac{k}{k_0}) + \frac{1}{6}\beta_s [\ln(\frac{k}{k_0})]^2}, \qquad (2.3)$$

where A_s is the amplitude at the pivot scale k_0, and n_s is the spectral index. We fix the pivot scale as $k_0 = 0.05\ \mathrm{Mpc}^{-1}$ as the Planck collaboration adopted [32]. To simplify the following analysis, we fix the ΛCDM parameters with the Planck 2018 best-fitted values [32], although we vary several
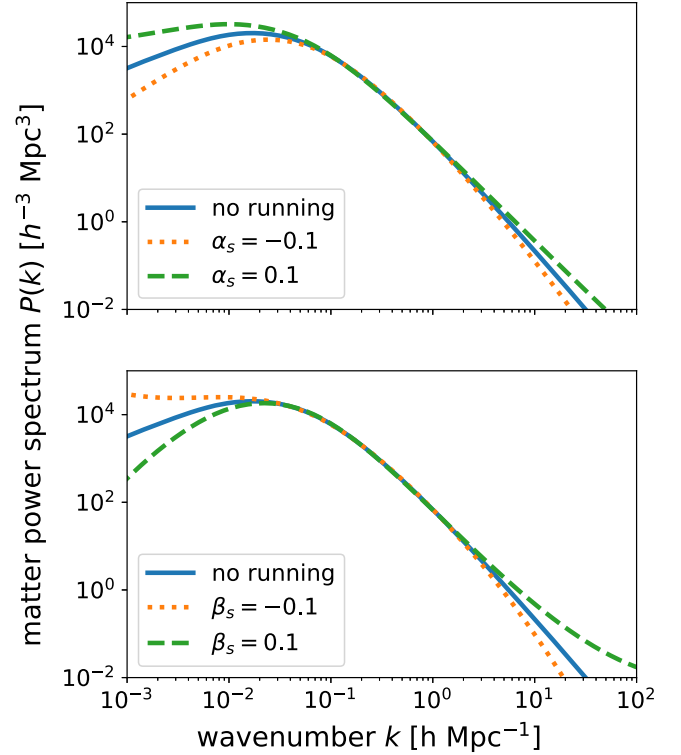
FIG. 3. Effects of the running spectral indices α_s and β_s on the matter power spectra.

astrophysical parameters as we describe below since the reionization history is more affected by astrophysical processes. Figure 3 shows the matter power spectra with varying running parameters. Here, the larger α_s and β_s enhance the small-scale power spectrum. However, on large scales, the larger α_s enhances the power spectrum as well, but the larger β_s reduces the large-scale matter power spectrum. Although cosmological observations such as CMB and LSS can probe large-scale fluctuations, constraints from such observations show the degeneracy between α_s and β_s. However, the combined analysis with other observations especially probing the small-scale fluctuations is expected to break such a degeneracy. In this paper, we focus on the reionization history as such a cosmological probe for the running spectral indices. Figure 4 shows the time evolution of the free electron fraction with different running parameters. Increasing α_s and β_s enhances the amplitude of small-scale matter fluctuations, and thereby high-redshift halo formation is promoted and the reionization gets earlier.

When calculating the reionization history, we use the astrophysical parameters adopted in the 21cmFAST version 2 [34].[1] In particular, three parameters $f_{*,10}$, $f_{esc,10}$, and M_{turn} give a significant impact on the reionizaiton

---

[1]The latest version of 21cmFAST is 3.2.1 (updated September 13, 2023), which has improved calculation speed and numerical stability. However, version 2 is slightly easier in extension and does not affect the calculation results. Therefore, we use version 2 in this paper.
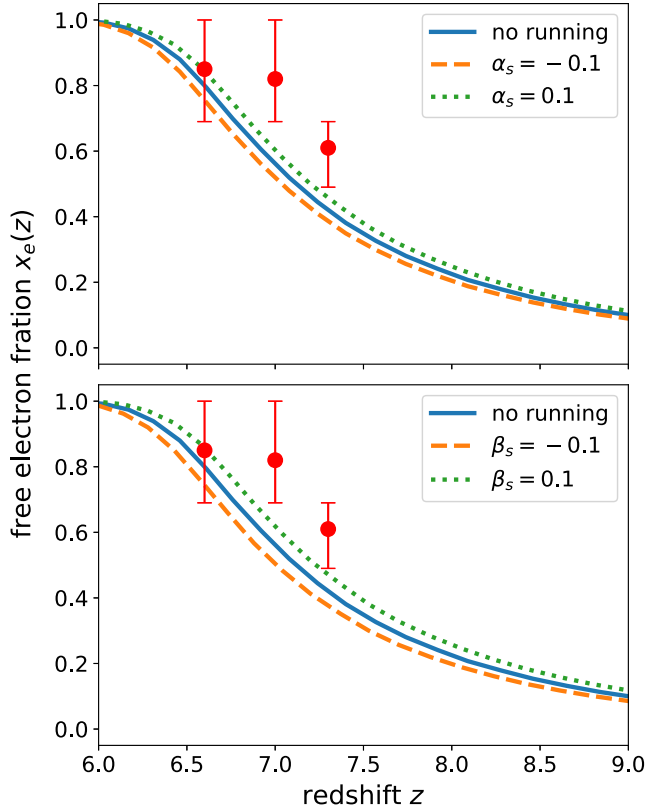
FIG. 4. Effects of the running spectral indices α_s and β_s on the reionization history. Astrophysical parameters are assumed to be the best-fitted values from HERA constraints [35]. Although the HERA best-fitted model slightly deviates from the SILVER-RUSH constraints, taking account of the uncertainties, the HERA results are consistent with the SILVERRUSH (see Fig. 5).

FIG. 5. Reionization history calculated by 21cmFAST with varying astrophysical parameters, $f_{*,10}$, $f_{\rm esc,10}$, and $M_{\rm turn}$, from top to bottom. The values for these parameters assumed here (shown inside the figure) correspond to the mean, 1σ upper and lower values from the HERA results [35].

history. These model parameters are defined by the stellar mass-to-baryon mass fraction in halos

$$f_*(M_{\rm halo}) = f_{*,10}\left(\frac{M_{\rm halo}}{10^{10}M_\odot}\right)^{\alpha_*}, \qquad (2.4)$$

the halo mass-dependent escape fraction of the ionizing photons

$$f_{\rm esc}(M_{\rm halo}) = f_{\rm esc,10}\left(\frac{M_{\rm halo}}{10^{10}M_\odot}\right)^{\alpha_{\rm esc}}, \qquad (2.5)$$

and the duty cycle of the star-forming galaxy

$$f_{\rm duty}(M_{\rm halo}) = \exp\left(-\frac{M_{\rm turn}}{M_{\rm halo}}\right), \qquad (2.6)$$

where α_* and $\alpha_{\rm esc}$ represent their power-law dependence. Figure 5 shows the time evolution of the free electron fraction with different astrophysical parameters, $f_{*,10}$, $f_{\rm esc,10}$, and $M_{\rm turn}$. Other astrophysical parameters are set to the best-fitted values of HERA results [35] as $\alpha_* = 0.50$, $\alpha_{\rm esc} = 0.02$, $t_* = 0.60$, $L_{\rm X}/{\rm SFR} = 10^{40.64}$ erg/s/$M_\odot$ yr. These parameters can also affect the reionization history. The effects on the free

electron fraction at $z = 7.3$ are $\Delta x_{\rm e} \lesssim 0.01$ for varying t_*, $\Delta x_{\rm e} \lesssim 0.05$ for varying $L_{\rm X}/{\rm SFR}$. Thus, these effects are smaller than the above three, $f_{*,10}$, $f_{\rm esc,10}$, and $M_{\rm turn}$. On the other hand, $\Delta x_{\rm e}$ can be larger than 0.1 for varying α_* and $\alpha_{\rm esc}$. However, we only use the free electron fraction at $z = 7.3$, and it is difficult to constrain the α_* and $\alpha_{\rm esc}$ independently of $f_{*,10}$ and $f_{\rm esc,10}$, respectively. Thus, we also fix α_* and $\alpha_{\rm esc}$. For the simulation parameters in 21cmFAST, we take such that the box size is $(400 \text{ Mpc})^3$, spatial resolution is 800^3 for high-resolution calculation, and 200^3 for low-resolution.

Our extended 21cmFAST enables us to calculate the reionization history varying the primordial running spectral indices and astrophysical parameters. However, the parameter inference with MCMC analysis, which is widely used to obtain constraints in cosmology and reionization [35–38], requires computational resources so much.[2] To save the

---

[2]In Ref. [39], using 21CMMC [36], they performed an MCMC analysis with varying two astrophysical parameters and two parameters related to the bumplike features of the primordial power spectrum. They have used the Planck optical depth constraint to perform the MCMC analysis but have not discussed other observations of reionization.

TABLE I.   Comparison between the free electron fraction calculated with the extended 21cmFAST code and our fitting function Eq. (2.8). The average value of the absolute difference between the 21cmFAST and Eq. (2.8) is about 0.02 among the parameter sets we used.

α_s	β_s	$f_{\text{esc},10}$	$f_{*,10}$	$M_{\text{turn}}/10^8 M_\odot$	$x_{\text{e}}^{\text{sim}}(z=7.3)$	$x_{\text{e}}^{\text{fit}}(z=7.3)$	Δx_{e}
0.002	0.031	0.074	0.055	10.240	0.442	0.451	−0.009
−0.038	0.015	0.113	0.067	3.857	0.688	0.650	0.038
−0.005	−0.013	0.124	0.067	3.788	0.748	0.705	0.042
−0.034	−0.000	0.064	0.087	6.155	0.383	0.409	−0.025
0.017	−0.030	0.100	0.079	4.691	0.688	0.645	0.043
0.032	0.039	0.050	0.068	2.139	0.684	0.676	0.008
0.007	−0.002	0.086	0.074	2.164	0.718	0.704	0.014
0.005	0.019	0.166	0.033	2.845	0.730	0.724	0.007
0.011	0.011	0.149	0.042	5.242	0.729	0.666	0.063
0.009	−0.018	0.100	0.055	5.932	0.447	0.437	0.011

calculation time, we construct the fitting function for the free electron fraction at redshift $z = 7.3$, based on our extended 21cmFAST results. Here, we use the free electron fraction only at $z = 7.3$, at which the most stringent constraint is given by the SILVERRUSH data. The fitting function that we obtained is

$$x_{\text{e}}(z = 7.3) = \min(1.0, \tilde{x}_{\text{e},7.3}), \qquad (2.7)$$

where

$$\tilde{x}_{\text{e},7.3} = \left\{ 0.421 \text{e}^A + B\left[\left(\frac{f_{*,10}}{0.058} \right)^C - 1.0 \right] \right.$$
$$\left. + D \log\left(\frac{M_{\text{turn}}}{3.8 \times 10^8 M_\odot} \right) \right\} \left(\frac{f_{\text{esc},10}}{0.078} \right)^E, \qquad (2.8)$$

with

$$A = 8.43\alpha_s + 11.41\beta_s,$$
$$B = 4.00\alpha_s + 7.75\beta_s + 0.38,$$
$$C = -5.24\alpha_s - 12.04\beta_s + 1.34,$$
$$D = -0.7\alpha_s - 1.20\beta_s - 0.07,$$
$$E = -3.11\beta_s + 1.08.$$

In order to check the validity of our fitting function, we performed test calculations with the random parameter sets (α_s, β_s, $f_{\text{esc},10}$, $f_{*,10}$, M_{turn}) in the ranges of $\alpha_s = (-0.05, 0.05)$, $\beta_s = (-0.05, 0.05)$, $f_{\text{esc},10} = (0.03, 0.3)$, $f_{*,10} = (0.024, 0.091)$, and $M_{\text{turn}}/M_\odot = (1.6 \times 10^8, 1.5 \times 10^9)$. We show the comparison between the extended 21cmFAST results and the fitting function in Table I. The absolute value of the average difference of the free electron fraction between that from 21cmFAST and the fitting function Δx_{e} is about 0.02, which is well smaller than the error in the SILVERRUSH data. Therefore, we can safely use our fitting function to analyze the constraint. Our fitting function (2.8) is obtained from the simulation data from

21cmFAST with $\alpha_s = (-0.015, 0.02)$, $\beta_s = (-0.015, 0.02)$, $f_{\text{esc},10} = (0.03, 0.3)$, $f_{*,10} = (0.024, 0.091)$, $M_{\text{turn}}/M_\odot = (1.6 \times 10^8, 1.5 \times 10^9)$. However, as seen in the results of Table I, the fitting function can also be applied outside the range of parameters that we used. Although one may expect that we can also use other parameters such as n_s, α_*, α_{esc} to improve the accuracy of our fitting function, it turns out that the inclusion of more parameters in the fitting does not help much. Therefore, we decided to fix other parameters to obtain the fitting function.

C. Constraints from the SILVERRUSH observation

In this study, we perform MCMC analysis, using the public code EMCEE [40], by comparing the SILVERRUSH results with Eq. (2.8) using a Gaussian likelihood. We use two priors on the running parameters: the flat one with $\alpha_s = (-0.1, 0.1)$, $\beta_s = (-0.1, 0.1)$ and the Gaussian Planck prior. The Planck prior assumes the two-dimensional Gaussian distribution function with the mean $\alpha_s = 0.0012$, $\beta_s = 0.0119$ and the covariance matrix from the Planck Legacy Archive [41]. Three astrophysical parameters are varied with flat priors as $f_{\text{esc},10} = (0.03, 0.3)$, $f_{*,10} = (0.024, 0.091)$, and $\log_{10}(M_{\text{turn}}/M_\odot) = (8.2, 9.2)$, which correspond to the 1σ uncertainty range from the HERA result [35].

First, we show constraints on α_s and β_s for the case that the astrophysical parameters are fixed as $f_{\text{esc},10} = 0.078$, $f_{*,10} = 0.058$, and $\log_{10}(M_{\text{turn}}/M_\odot) = 8.58$, which are taken from the recent HERA best-fitted values in Fig. 6. When imposing the flat priors for α_s and β_s, a strong degeneracy between α_s and β_s appears. This degeneracy shows a negative correlation because the reionization redshift is considered to be determined by the small-scale matter power spectrum where effects of α_s and β_s are canceled. On the other hand, CMB anisotropies probe large-scale perturbations, and therefore, the direction of the degeneracy is positive since the response of large-scale fluctuations to the change of α_s and β_s is opposite to that of
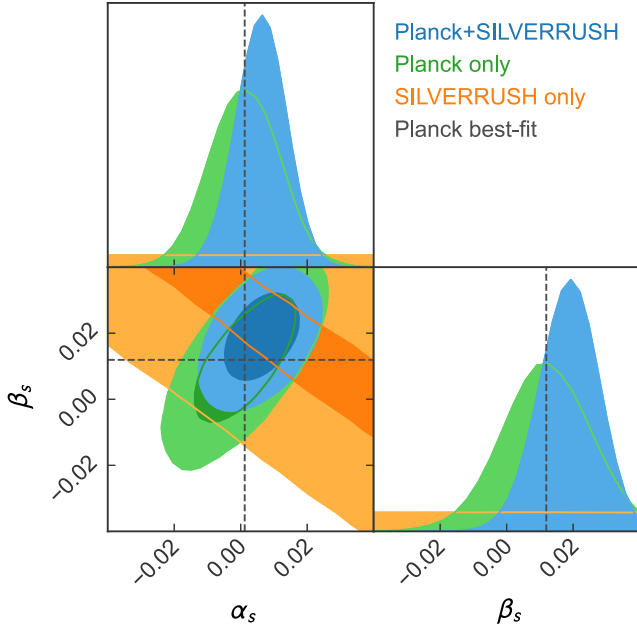
FIG. 6. Triangle plot of constraints on (α_s, β_s) from observations of the reionization history. The constraint with the flat prior on (α_s, β_s) is labeled as "SILVERRUSH only" (orange), and one with the Gaussian Planck prior is labeled as "Planck+ SILVERRUSH" (blue). For comparison, the constraint obtained from Planck results is also shown as "Planck only" (green) [1,41].

small-scale as seen from Fig. 3. Figure 6 shows that combining CMB and reionization observations can break these degeneracies and bring stringent constraints on α_s and β_s.
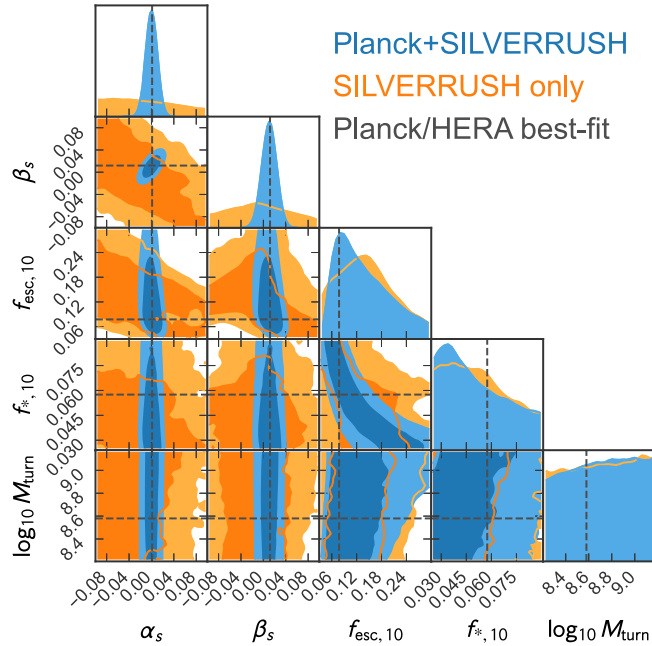
FIG. 7. Triangle plot of constraint on $(\alpha_s, \beta_s, f_{*,10}, f_{esc,10}, M_{turn})$ from the SILVERRUSH observations with the flat prior on (α_s, β_s) (orange), and that with the Gaussian Planck prior [41] (blue).

TABLE II. The best-fit values and 68% C.L. errors for the running and astrophysical parameters from SILVERRUSH observations.

	Without astrophysical parameters		With astrophysical parameters	
	Flat prior	Planck prior	Flat prior	Planck prior
α_s	$\cdots$	$0.006^{+0.007}_{-0.007}$	$-0.048^{+0.149}_{-0.103}$	$0.001^{+0.010}_{-0.010}$
β_s	$\cdots$	$0.019^{+0.008}_{-0.009}$	$0.048^{+0.110}_{-0.118}$	$0.012^{+0.013}_{-0.013}$
$f_{esc,10}$			$0.087^{+0.147}_{-0.064}$	$0.112^{+0.055}_{-0.041}$
$f_{*,10}$			$0.104^{+0.182}_{-0.072}$	$0.064^{+0.022}_{-0.024}$
$\log_{10}(M_{turn}/M_\odot)$			$9.148^{+0.937}_{-1.370}$	$9.053^{+0.912}_{-0.737}$

When one discusses the constraints on the running spectral indices from the reionization history, the degeneracies between the running and astrophysical parameters should be considered. Figure 7 shows the results of MCMC analysis when all parameters are sampled. When we assume a flat prior on α_s and β_s, although one can see a weak correlation between α_s and β_s, most parameters are poorly constrained and the 68% C.L. errors on the running spectral indices are $\Delta\alpha_s \sim \Delta\beta_s \sim \mathcal{O}(0.1)$. On the other hand, when we impose the Planck prior for α_s and β_s, the constraints become significantly improved as $\Delta\alpha_s \sim \Delta\beta_s \sim 0.01$, while constraints on astrophysical parameters are not changed much between those for the two different priors. Furthermore, we found that $f_{esc,10}$ and $f_{*,10}$ are slightly more sensitive to the reionization history, compared with M_{turn} as expected from Fig. 5. In Table II, we summarize the best-fit values and 68% C.L. errors for two prior cases with and without fixing astrophysical parameters.

D. Effects of the redshift width of reionization Δz

So far, we have fixed the redshift width of tanh-type reionization as $\Delta z = 0.5$. Here, we compare the MCMC analyses with fixed Δz and with varied Δz. In the analysis so far, we used only one redshift data point for SILVERRUSH, as $0.49 \leq x_e \leq 0.69$ at $z = 7.3$. When fixing all the parameters, the free electron fraction at $z = 7.3$ is determined by using Eqs. (2.7) and (2.8). Since the analysis with only one redshift data cannot constrain the effect of varying Δz, we use three different redshift data-points of SILVERRUSH survey, as $x_e \geq 0.69$ at $z = 6.6$, $x_e \geq 0.69$ at $z = 7.0$, and $0.49 \leq x_e \leq 0.69$ at $z = 7.3$ in this section. In the MCMC analysis with varied Δz, after determining the x_e at $z = 7.3$ by choosing model parameters $(\alpha_s, \beta_s, f_{*,10}, f_{esc,10}, M_{turn})$, the x_e at the other redshifts (i.e., at $z = 6.6$ and $z = 7.0$) can be determined by giving $x_e(z = 7.3)$ and Δz based on the tanh-type function (2.1). For reference, we show the reionization history with different Δz in Fig. 8. This figure shows that the additional two data points may be useful to constrain the width of reionization Δz.
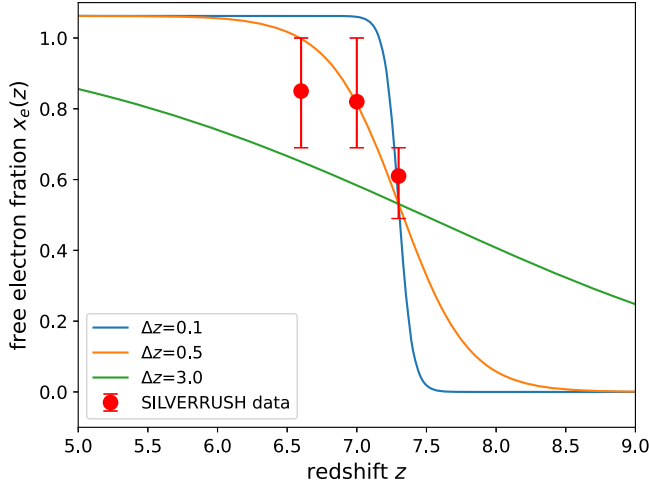
FIG. 8.   Reionization history with different values of $\Delta z = 0.1$, 0.5, and 3.0. For all cases, the free electron fraction at $z = 7.3$ is fixed at $x_e(z = 7.3) = 0.5$.

In the analysis with varied Δz, we impose the flat prior distribution as $\Delta z = (0.1, 3.0)$. This prior choice is motivated by the following reasons. The observation of the kinetic Sunyaev-Zel'dovich effect indicates $\Delta z < 0.79$ at 95% C.L. [42]. On the other hand, the radiation-hydrodynamic (RHD) simulation predicts relatively higher values of $\Delta z \sim 1.5$–2.5 [43]. It should be noted that, however, since the RHD simulation results do not follow the tanh-type redshift evolution, it is not straightforward to convert their results to the constraints on Δz. Therefore, we adopt a conservative prior on the Δz.
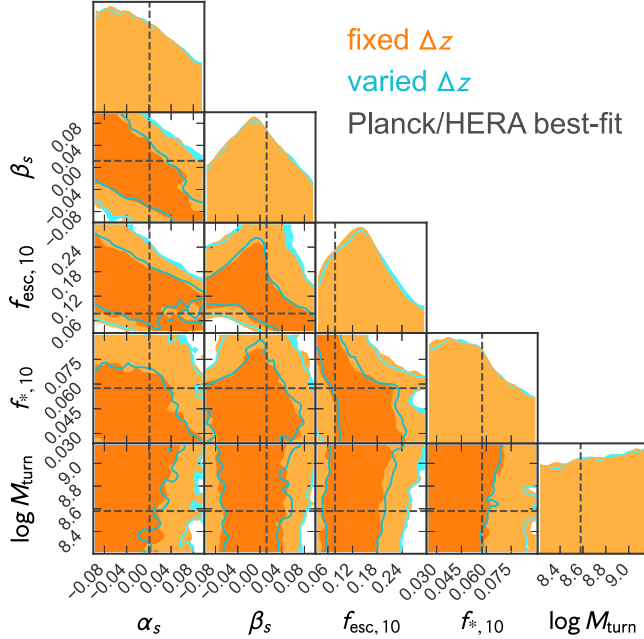
FIG. 9.   Triangle plot of constraint on $(\alpha_s, \beta_s, f_{*,10}, f_{esc,10}, M_{turn})$ from the SILVERRUSH observations with Δz being fixed (blue) and varied (orange). Here, we assume a flat prior for all parameters.
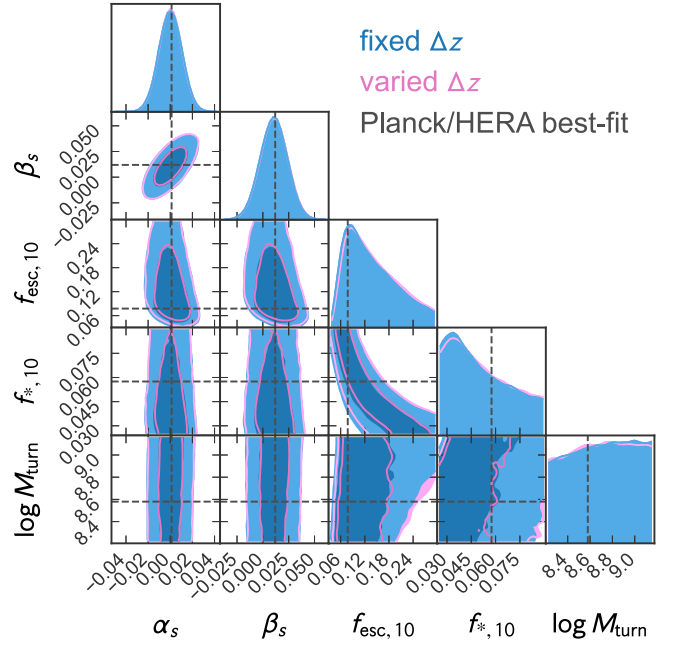
FIG. 10.   Triangle plot of constraint on $(\alpha_s, \beta_s, f_{*,10}, f_{esc,10}, M_{turn})$ from the SILVERRUSH observations with Δz being fixed (blue) and varied (orange). Here, we assume the Gaussian Planck prior for α_s and β_s, but a flat prior on other parameters.

Figure 9 shows the comparison of constraints from SILVERRUSH observations with flat priors on all parameters $(\alpha_s, \beta_s, f_{*,10}, f_{esc,10}, M_{turn})$, with Δz being fixed and varied. We found that Δz is constrained as $\Delta z = 1.327^{+1.056}_{-0.754}$ at 68% C.L. Constraints on the other parameters in the analysis with and without varied Δz are almost the same. In Fig. 10, we show the case with the Gaussian Planck prior on (α_s, β_s), but with a flat prior for the others $(f_{*,10}, f_{esc,10}, M_{turn})$. In this analysis, we obtained $\Delta z = 1.339^{+1.043}_{-0.767}$ at 68% C.L., and constraints on other parameters are almost unchanged even when we vary Δz as in Fig. 9. From the results of Figs. 9 and 10, we can conclude that varying redshift width of reionization Δz does not give a significant impact on the constraints on the primordial fluctuations in our analysis.

III. CONCLUSION

In this work, we have argued that the reionization history can be used as a novel probe of primordial fluctuations. To this end, we have investigated the impact of the small-scale primordial curvature perturbations on the reionization history. We modified the seminumerical simulation code 21cmFAST to examine the reionization history incorporating the running of the spectral indices of the primordial power spectrum up to the second order. Based on calculations with 21cmFAST, we constructed the fitting function for the free electron fraction at $z = 7.3$. We also performed the MCMC analysis by using the fitting function and observational data

of the reionization history from the SILVERRUSH LAEs to obtain the constraints on the running spectral indices. In case the astrophysical uncertainties are neglected, the running spectral indices can be strongly constrained by combining the observation of the reionization history and that of CMB. On the other hand, when considering uncertainties of the astrophysical parameters as inferred in the recent 21-cm observations [35], we found that the current observational constraints on the reionization history cannot severely constrain the running spectral indices. This result is based on the relatively simple astrophysical model, which is adopted in the 21cmFAST. Therefore, if one considers a more complicated astrophysical model, the constraints on the running parameters would get looser. However, in near future, the measurements of astrophysical parameters can become more precise and, in such a case, the reionization history would be a useful probe of primordial fluctuations and can augment other methods to severely constrain them.

Finally, we comment on the other observations of the reionization history. In this work, we mainly used the free electron fraction derived from the luminosity function of the LAEs observed in the SILVERRUSH survey. Our choice of observational data is just to demonstrate the power of constraining primordial perturbations using the reionization history. Actually, many observational constraints on the reionization history are reported, such as the Ly-α equivalent width of the Lyman break galaxies (LBGs) [44–47], the number fraction of LBGs emitting Ly-α in all observed LBGs [48], gamma-ray burst and the QSO damping wings [49–54], the Ly-α and Ly-β forest dark gaps of QSO spectra [55,56], and the Gunn-Peterson trough of QSOs [57,58]. These observational data are independent but some of the above results show inconsistencies (for examples, see Fig. 11 of Ref. [30]). Among them, the reionization history obtained by the LAE luminosity function with the Subaru telescope that we used in this work provides constraints at different redshifts, and they are consistent with each other [30,59–62]. It is worth noting that measurements of the LAE luminosity function using other telescopes provide different constraints on the reionization history [63,64], and therefore, the best-fit values in our analysis may depend on the observational data choice.

The current observational constraint errors on the free electron fractions are $\Delta x_{\rm e} \sim \mathcal{O}(0.1)$. However, we would expect that more precise measurements of the reionization history can decrease the uncertainties on cosmological and astrophysical parameters. However, it may be difficult to resolve degeneracies among the parameters in our analysis, i.e., α_s, β_s, $f_{*,10}$, $f_{\rm esc,10}$, and $M_{\rm turn}$ by using observations of the reionization history only. Further improvement on the constraints on the primordial curvature perturbations is expected to be obtained by combining other types of observations, such as the recent high-redshift galaxy luminosity function obtained by the James Webb Space Telescope [65–67], which is worth investigating. We leave this issue to future work.

ACKNOWLEDGMENTS

[1] Y. Akrami *et al.* (Planck Collaboration), Planck 2018 results. X. Constraints on inflation, Astron. Astrophys. **641,** A10 (2020).

[2] C. Hikage *et al.* (HSC Collaboration), Cosmology from cosmic shear power spectra with Subaru Hyper Suprime-Cam first-year data, Publ. Astron. Soc. Jpn. **71,** 43 (2019).

[3] C. Heymans *et al.* (KiDS Collaboration), KiDS-1000 Cosmology: Multi-probe weak gravitational lensing and spectroscopic galaxy clustering constraints, Astron. Astrophys. **646,** A140 (2021).

[4] T. M. C. Abbott *et al.* (DES Collaboration), Dark energy survey year 3 results: Cosmological constraints from galaxy clustering and weak lensing, Phys. Rev. D **105,** 023520 (2022).

[5] N. Palanque-Delabrouille, C. Yèche, N. Schöneberg, J. Lesgourgues, M. Walther, S. Chabanier, and E. Armengaud, Hints, neutrino bounds, and WDM constraints from SDSS DR14 Lyman-α and Planck full-survey data, J. Cosmol. Astropart. Phys. 04 (2020) 038.

[6] S. Alam *et al.* (SDSS Collaboration), Completed SDSS-IV extended Baryon oscillation spectroscopic survey: Cosmological implications from two decades of spectroscopic surveys at the apache point observatory, Phys. Rev. D **103,** 083533 (2021).

[7] Abdurro'uf *et al.* (SDSS Collaboration), The seventeenth data release of the sloan digital sky surveys: Complete Release of MaNGA, MaStar, and APOGEE-2 data, Astrophys. J. Suppl. Ser. **259,** 35 (2022).

[8] S. Yoshiura, K. Takahashi, and T. Takahashi, Impact of EDGES 21-cm global signal on the primordial power spectrum, Phys. Rev. D **98,** 063529 (2018).

[9] S. Yoshiura, K. Takahashi, and T. Takahashi, Probing small scale primordial power spectrum with 21 cm line global signal, Phys. Rev. D **101,** 083520 (2020).

[10] Y. Mao, M. Tegmark, M. McQuinn, M. Zaldarriaga, and O. Zahn, How accurately can 21 cm tomography constrain cosmology?, Phys. Rev. D **78,** 023529 (2008).

[11] K. Kohri, Y. Oyama, T. Sekiguchi, and T. Takahashi, Precise measurements of primordial power spectrum with 21 cm fluctuations, J. Cosmol. Astropart. Phys. 10 (2013) 065.

[12] H. Shimabukuro, K. Ichiki, S. Inoue, and S. Yokoyama, Probing small-scale cosmological fluctuations with the 21 cm forest: Effects of neutrino mass, running spectral index, and warm dark matter, Phys. Rev. D **90,** 083003 (2014).

[13] S. Bird, H. V. Peiris, M. Viel, and L. Verde, Minimally parametric power spectrum reconstruction from the Lyman α forest, Mon. Not. R. Astron. Soc. **413,** 1717 (2011).

[14] N. Palanque-Delabrouille, C. Yèche, J. Baur, C. Magneville, G. Rossi, J. Lesgourgues, A. Borde, E. Burtin, J.-M. LeGoff, J. Rich, M. Viel, and D. Weinberg, Neutrino masses and cosmology with Lyman-alpha forest power spectrum, J. Cosmol. Astropart. Phys. 11 (2015) 011.

[15] T. Sekiguchi, T. Takahashi, H. Tashiro, and S. Yokoyama, 21 cm angular power spectrum from minihalos as a probe of primordial spectral runnings, J. Cosmol. Astropart. Phys. 02 (2018) 053.

[16] T. Bringmann, P. Scott, and Y. Akrami, Improved constraints on the primordial power spectrum at small scales from ultracompact minihalos, Phys. Rev. D **85,** 125027 (2012).

[17] T. Nakama, T. Suyama, K. Kohri, and N. Hiroshima, Constraints on small-scale primordial power by annihilation signals from extragalactic dark matter minihalos, Phys. Rev. D **97,** 023539 (2018).

[18] A. S. Josan, A. M. Green, and K. A. Malik, Generalized constraints on the curvature perturbation from primordial black holes, Phys. Rev. D **79,** 103520 (2009).

[19] G. Sato-Polito, E. D. Kovetz, and M. Kamionkowski, Constraints on the primordial curvature power spectrum from primordial black holes, Phys. Rev. D **100,** 063521 (2019).

[20] I. Ben-Dayan and R. Takahashi, Constraints on small-scale cosmological fluctuations from SNe lensing dispersion, Mon. Not. R. Astron. Soc. **455,** 552 (2016).

[21] W. Hu, D. Scott, and J. Silk, Power spectrum constraints from spectral distortions in the cosmic microwave background, Astrophys. J. Lett. **430,** L5 (1994).

[22] J. Chluba, R. Khatri, and R. A. Sunyaev, CMB at 2×2 order: The dissipation of primordial acoustic waves and the observable part of the associated energy release, Mon. Not. R. Astron. Soc. **425,** 1129 (2012).

[23] J. Chluba, A. L. Erickcek, and I. Ben-Dayan, Probing the inflaton: Small-scale power spectrum constraints from measurements of the cosmic microwave background energy spectrum, Astrophys. J. **758,** 76 (2012).

[24] R. Khatri and R. A. Sunyaev, Forecasts for CMB μ and i-type spectral distortion constraints on the primordial power spectrum on scales $8 \lesssim k \lesssim 10^4$ Mpc^{-1} with the future Pixie-like experiments, J. Cosmol. Astropart. Phys. 06 (2013) 026.

[25] S. Clesse, B. Garbrecht, and Y. Zhu, Testing inflation and curvaton scenarios with CMB distortions, J. Cosmol. Astropart. Phys. 10 (2014) 046.

[26] G. Cabass, E. Di Valentino, A. Melchiorri, E. Pajer, and J. Silk, Constraints on the running of the running of the scalar tilt from CMB anisotropies and spectral distortions, Phys. Rev. D **94,** 023523 (2016).

[27] K. Kainulainen, J. Leskinen, S. Nurmi, and T. Takahashi, CMB spectral distortions in generic two-field models, J. Cosmol. Astropart. Phys. 11 (2017) 002.

[28] S. Yoshiura, M. Oguri, K. Takahashi, and T. Takahashi, Constraints on primordial power spectrum from galaxy luminosity functions, Phys. Rev. D **102,** 083515 (2020).

[29] S. Ando, N. Hiroshima, and K. Ishiwata, Constraining the primordial curvature perturbation using dark matter substructure, Phys. Rev. D **106,** 103014 (2022).

[30] H. Goto, K. Shimasaku, S. Yamanaka, R. Momose, M. Ando, Y. Harikane, T. Hashimoto, A. K. Inoue, and M. Ouchi, SILVERRUSH. XI. Constraints on the Lyα luminosity function and cosmic reionization at $z = 7.3$ with Subaru/Hyper Suprime-Cam, Astrophys. J. **923,** 229 (2021).

[31] P. A. R. Ade et al. (Planck Collaboration), Planck 2015 results. XIII. Cosmological parameters, Astron. Astrophys. **594,** A13 (2016).

[32] N. Aghanim et al. (Planck Collaboration), Planck 2018 results. VI. Cosmological parameters, Astron. Astrophys. **641,** A6 (2020).

[33] A. Lewis, Cosmological parameters from WMAP 5-year temperature maps, Phys. Rev. D **78,** 023002 (2008).

[34] J. Park, A. Mesinger, B. Greig, and N. Gillet, Inferring the astrophysics of reionization and cosmic dawn from galaxy luminosity functions and the 21-cm signal, Mon. Not. R. Astron. Soc. **484,** 933 (2019).

[35] Z. Abdurashidova et al. (HERA Collaboration), HERA Phase I limits on the cosmic 21 cm signal: Constraints on astrophysics and cosmology during the epoch of reionization, Astrophys. J. **924,** 51 (2022).

[36] B. Greig and A. Mesinger, 21CMMC: An MCMC analysis tool enabling astrophysical parameter studies of the cosmic 21 cm signal, Mon. Not. R. Astron. Soc. **449,** 4246 (2015).

[37] J. B. Muñoz, C. Dvorkin, and F.-Y. Cyr-Racine, Probing the small-scale matter power spectrum with large-scale 21-cm data, Phys. Rev. D **101,** 063526 (2020).

[38] B. Greig, J. S. B. Wyithe, S. G. Murray, S. J. Mutch, and C. M. Trott, Generating extremely large-volume reionization simulations, Mon. Not. R. Astron. Soc. **516,** 5588 (2022).

[39] S. S. Naik, P. Chingangbam, and K. Furuuchi, Particle production during inflation: Constraints expected from redshifted 21 cm observations from the epoch of reionization, J. Cosmol. Astropart. Phys. 04 (2023) 058.

[40] D. Foreman-Mackey, D. W. Hogg, D. Lang, and J. Goodman, EMCEE: The MCMC hammer, Publ. Astron. Soc. Pac. **125,** 306 (2013).

[41] Planck legacy archive, https://pla.esac.esa.int/.

[42] R. Adam et al. (Planck Collaboration), Planck intermediate results. XLVII. Planck constraints on reionization history, Astron. Astrophys. **596,** A108 (2016).

[43] H. Trac, Parametrizing the reionization history with the redshift midpoint, duration, and asymmetry, Astrophys. J. Suppl. Ser. **858,** L11 (2018).

[44] C. A. Mason, T. Treu, M. Dijkstra, A. Mesinger, M. Trenti, L. Pentericci, S. de Barros, and E. Vanzella, The universe is reionizing at $z \sim 7$: Bayesian inference of the IGM neutral

fraction using Lyα emission from galaxies, Astrophys. J. **856,** 2 (2018).

[45] C. A. Mason, A. Fontana, T. Treu, K. B. Schmidt, A. Hoag, L. Abramson, R. Amorin, M. Bradač, L. Guaita, T. Jones, A. Henry, M. A. Malkan, L. Pentericci, M. Trenti, and E. Vanzella, Inferences on the timeline of reionization at $z \sim 8$ from the KMOS lens-amplified spectroscopic survey, Mon. Not. R. Astron. Soc. **485,** 3947 (2019).

[46] A. Hoag, M. Bradač, K. Huang, C. Mason, T. Treu, K. B. Schmidt, M. Trenti, V. Strait, B. C. Lemaux, E. Q. Finney, and M. Paddock, Constraining the neutral fraction of hydrogen in the IGM at redshift 7.5, Astrophys. J. **878,** 12 (2019).

[47] L. R. Whitler, C. A. Mason, K. Ren, M. Dijkstra, A. Mesinger, L. Pentericci, M. Trenti, and T. Treu, The impact of scatter in the galaxy UV luminosity to halo mass relation on Ly α visibility during the epoch of reionization, Mon. Not. R. Astron. Soc. **495,** 3602 (2020).

[48] A. Mesinger, A. Aykutalp, E. Vanzella, L. Pentericci, A. Ferrara, and M. Dijkstra, Can the intergalactic medium cause a rapid drop in Lyα emission at $z > 6$?, Mon. Not. R. Astron. Soc. **446,** 566 (2015).

[49] T. Totani, N. Kawai, G. Kosugi, K. Aoki, T. Yamada, M. Iye, K. Ohta, and T. Hattori, Implications for cosmic reionization from the optical afterglow spectrum of the gamma-ray burst 050904 at $z = 6.3^*$, Publ. Astron. Soc. Jpn. **58,** 485 (2006).

[50] T. Totani, K. Aoki, T. Hattori, G. Kosugi, Y. Niino, T. Hashimoto, N. Kawai, K. Ohta, T. Sakamoto, and T. Yamada, Probing intergalactic neutral hydrogen by the Lyman alpha red damping wing of gamma-ray burst 130606A afterglow spectrum at $z = 5.913$, Publ. Astron. Soc. Jpn. **66,** 63 (2014).

[51] J. Schroeder, A. Mesinger, and Z. Haiman, Evidence of Gunn-Peterson damping wings in high-z quasar spectra: Strengthening the case for incomplete reionization at $z \sim 6$–7, Mon. Not. R. Astron. Soc. **428,** 3058 (2013).

[52] F. B. Davies, J. F. Hennawi, E. Bañados, Z. Lukić, R. Decarli, X. Fan, E. P. Farina, C. Mazzucchelli, H.-W. Rix, B. P. Venemans, F. Walter, F. Wang, and J. Yang, Quantitative constraints on the reionization history from the IGM damping wing signature in two quasars at $z > 7$, Astrophys. J. **864,** 142 (2018).

[53] B. Greig, A. Mesinger, and E. Bañados, Constraints on reionization from the $z = 7.5$ QSO ULASJ1342 + 0928, Mon. Not. R. Astron. Soc. **484,** 5094 (2019).

[54] F. Wang, F. B. Davies, J. Yang, J. F. Hennawi, X. Fan, A. J. Barth, L. Jiang, X.-B. Wu, D. M. Mudd, E. Bañados, F. Bian, R. Decarli, A.-C. Eilers, E. P. Farina, B. Venemans, F. Walter, and M. Yue, A significantly neutral intergalactic medium around the luminous $z = 7$ quasar J0252-0503, Astrophys. J. **896,** 23 (2020).

[55] I. D. McGreer, A. Mesinger, and V. D'Odorico, Model-independent evidence in favour of an end to reionization by $z \approx 6$, Mon. Not. R. Astron. Soc. **447,** 499 (2015).

[56] Y. Zhu *et al.*, Long dark gaps in the Lyβ forest at $z < 6$: Evidence of ultra-late reionization from XQR-30 spectra, Astrophys. J. **932,** 76 (2022).

[57] X. Fan, M. A. Strauss, R. H. Becker, R. L. White, J. E. Gunn, G. R. Knapp, G. T. Richards, D. P. Schneider, J. Brinkmann, and M. Fukugita, Constraining the evolution of the ionizing background and the epoch of reionization with

$z \sim 6$ quasars. II. A sample of 19 quasars, Astron. J. **132,** 117 (2006).

[58] T. Goto, Y. Utsumi, T. Hattori, S. Miyazaki, and C. Yamauchi, A Gunn-Peterson test with a QSO at $z = 6.4$, Mon. Not. R. Astron. Soc. **415,** L1 (2011).

[59] A. Konno, M. Ouchi, Y. Ono, K. Shimasaku, T. Shibuya, H. Furusawa, K. Nakajima, Y. Naito, R. Momose, S. Yuma, and M. Iye, Accelerated evolution of the Lyα luminosity function at $z > 7$ revealed by the subaru ultra-deep survey for Lyα emitters at $z = 7.3$, Astrophys. J. **797,** 16 (2014).

[60] A. K. Inoue, K. Hasegawa, T. Ishiyama, H. Yajima, I. Shimizu, M. Umemura, A. Konno, Y. Harikane, T. Shibuya, M. Ouchi, K. Shimasaku, Y. Ono, H. Kusakabe, R. Higuchi, and C.-H. Lee, SILVERRUSH. VI. A simulation of Lyα emitters in the reionization epoch and a comparison with Subaru Hyper Suprime-Cam survey early data, Publ. Astron. Soc. Jpn. **70,** 55 (2018).

[61] R. Itoh, M. Ouchi, H. Zhang, A. K. Inoue, K. Mawatari, T. Shibuya, Y. Harikane, Y. Ono, H. Kusakabe, K. Shimasaku, S. Fujimoto, I. Iwata, M. Kajisawa, N. Kashikawa, S. Kawanomoto, Y. Komiyama, C.-H. Lee, T. Nagao, and Y. Taniguchi, CHORUS. II. Subaru/HSC determination of the Lyα luminosity function at $z = 7.0$: Constraints on cosmic reionization model parameter, Astrophys. J. **867,** 46 (2018).

[62] A. Konno, M. Ouchi, T. Shibuya, Y. Ono, K. Shimasaku, Y. Taniguchi, T. Nagao, M. A. R. Kobayashi, M. Kajisawa, N. Kashikawa, A. K. Inoue, M. Oguri, H. Furusawa, T. Goto, Y. Harikane, R. Higuchi, Y. Komiyama, H. Kusakabe, S. Miyazaki, K. Nakajima, and S.-Y. Wang, SILVERRUSH. IV. Lyα luminosity functions at $z = 5.7$ and 6.6 studied with ~ 1300 Lyα emitters on the 14–21 deg^2 sky, Publ. Astron. Soc. Jpn. **70,** S16 (2018).

[63] W. Hu, J. Wang, Z.-Y. Zheng, S. Malhotra, J. E. Rhoads, L. Infante, L. F. Barrientos, H. Yang, C. Jiang, W. Kang, L. A. Perez, I. Wold, P. Hibon, L. Jiang, A. A. Khostovan, F. Valdes, A. R. Walker, G. Galaz, A. Coughlin, S. Harish, X. Kong, J. Pharo, and X. Zheng, The Lyα luminosity function and cosmic reionization at $z \sim 7.0$: A tale of two LAGER fields, Astrophys. J. **886,** 90 (2019).

[64] A. M. Morales, C. A. Mason, S. Bruton, M. Gronke, F. Haardt, and C. Scarlata, The evolution of the Lyman-alpha luminosity function during reionization, Astrophys. J. **919,** 120 (2021).

[65] I. Labbe, P. van Dokkum, E. Nelson, R. Bezanson, K. Suess, J. Leja, G. Brammer, K. Whitaker, E. Mathews, M. Stefanon, and B. Wang, A population of red candidate massive galaxies 600 Myr after the Big Bang, Nature (London) **616,** 266 (2023).

[66] R. Endsley, D. P. Stark, L. Whitler, M. W. Topping, Z. Chen, A. Plat, J. Chisholm, and S. Charlot, A JWST/NIRCam study of key contributors to reionization: The star-forming and ionizing properties of UV-faint $z \sim 7$–8 galaxies, Mon. Not. R. Astron. Soc. **524,** 2312 (2023).

[67] N. J. Adams, C. J. Conselice, L. Ferreira, D. Austin, J. A. A. Trussler, I. Juodžbalis, S. M. Wilkins, J. Caruana, P. Dayal, A. Verma, and A. P. Vijayan, Discovery and properties of ultra-high redshift galaxies ($9 < z < 12$) in the JWST ERO SMACS 0723 field, Mon. Not. R. Astron. Soc. **518,** 4755 (2023).